

Simulation of the Intraseasonal Variance of the South American Summer Monsoon

VASUBANDHU MISRA

Center for Ocean–Land–Atmosphere Studies, Institute of Global Environment and Society, Inc., Calverton, Maryland

(Manuscript received 13 November 2003, in final form 2 August 2004)

ABSTRACT

This study reveals the inadequacy of the Center for Ocean–Land–Atmosphere Studies (COLA) atmospheric general circulation model (AGCM) and the National Centers for Environmental Prediction–National Center for Atmospheric Research (NCEP–NCAR) reanalysis to resolve the variance of the intraseasonal anomalies of outgoing longwave radiation (OLR) over the South American summer monsoon (SASM) domain and the equatorial eastern Pacific Ocean (EEPO) owing to their coarse horizontal resolution. However, when the NCEP–NCAR reanalysis is downscaled by roughly a factor of 2.5 using the Regional Spectral Model (RSM; control-A experiment), the simulation of the seasonal mean variance of intraseasonal anomalies of OLR improves significantly. But downscaling the results of the COLA AGCM (control-B experiment) by roughly a factor of 4 led to no further improvement.

Using the novel technique of anomaly nesting, which replaces the climatology of the COLA AGCM of the nested variables at the lateral boundaries of the RSM with the NCEP–NCAR reanalysis climatology (AN experiment), the simulation of the intraseasonal variance of OLR improves significantly over control-B runs. This improvement is shown to coincide with a distinct diurnal variation of the intraseasonal scales displayed in the AN integrations, which compare reasonably well with control-A integrations. A disappointing result of this study is that the generated variance of intraseasonal anomalies of OLR in the AN integrations arises from the internal variability of the model. However, it is concluded that the systematic errors of the COLA AGCM imposed on RSM from the lateral boundary conditions suppress the generation of intraseasonal variability.

1. Introduction

The Madden–Julian oscillation (MJO) has been a topic of significant interest, especially in the recent context of connecting weather with seasonal climate prediction (Waliser et al. 2003b). The association of this oscillation with a wide range of phenomenon, such as the active and break periods of the Asian–Australian monsoons (Lau and Chan 1986; Hendon and Liebmann 1990), El Niño–Southern Oscillation (ENSO; Kessler and Kleeman 2000), and anomalies of the South American summer monsoon (SASM; Paegle and Mo 1997; Jones and Carvalho 2002) also make this oscillation important. The observed see-saw pattern of the OLR anomalies between the South Atlantic convergence zone (SACZ) and the subtropical plains of South America typically on the 20–40-day time scale has been shown to be quite robust (Paegle and Mo 1997; Paegle et al. 2000). Previous studies indicate that when the SACZ is anomalously wet (dry) then the subtropical

plains of South America are concomitantly dry (wet). Paegle et al. (2000) show two distinct scales of variability with periods of 36–40 days and 22–28 days. They show that the former is related to MJO with OLR anomalies propagating eastward from the western Pacific. They further show that both these oscillations contribute to the observed dipole pattern between the SACZ and the subtropical plains of South America. Other teleconnection studies also indicate that the intraseasonal variability over the SACZ region can be linked to the MJO over the South Pacific convergence zone (SPCZ) by Rossby wave propagation (Kiladis and Weickmann 1992; Grimm and Silva Dias 1995). Despite the robust prevalence of the MJO and the global teleconnections that it facilitates, the prediction of this oscillation is intriguingly poor (Slingo et al. 1996; Sperber et al. 2001; Waliser et al. 2003a). The general conclusion is that most current atmospheric general circulation models (AGCMs) have difficulty in simulating the MJO in terms of amplitude, propagation, and spatial pattern, and even the associated seasonal and interannual variance. Consequently, the associated covariability of the MJO with the SASM and the Asian–Australian monsoon is also affected in these AGCMs. Waliser et al. (2003b) concluded from a set of idealized (twin predictability) experiments, conducted with an

Corresponding author address: Vasubandhu Misra, Center for Ocean–Land–Atmosphere Studies, Institute of Global Environment and Society, Inc., 4041 Powder Mill Road, Suite 302, Calverton, MD 20705.
E-mail: misra@cola.iges.org

AGCM that simulated a relatively realistic MJO, that useful predictability of MJO extends to about 25–30 days for velocity potential and 10–15 days for rainfall.

Although the circulation in the eastern equatorial Pacific Ocean region (EEPO) is not identified as part of the SASM (Zhou and Lau 1998) it exerts a significant influence on the interannual variability of the SASM (Ropelewski and Halpert 1987; Misra et al. 2002b). Furthermore, Maloney and Kiehl (2002) show from observations that the circulation in the EEPO displays significant intraseasonal variance. Therefore, the EEPO is included along with the SASM in this analysis. It should also be mentioned that we will be examining intraseasonal variability only in the outgoing longwave radiation (OLR), as it has good observational coverage both temporally and spatially (Liebmann and Smith 1996) for validation. In addition, observational studies (Liebmann et al. 1999) and some of the model integrations of this study show robust intraseasonal variability in OLR over the region. Therefore the objectives of this study are as follows:

- To evaluate a variety of austral summer seasonal model runs (which includes both AGCM and regional climate models) for OLR variance at 20–40 days (henceforth intraseasonal) time scales.
- To assess the signal-to-noise ratio of this intraseasonal variance over the SASM and the EEPO domains.

It should be noted that all model runs in this study are integrated with prescribed observed sea surface temperature (SST). National Centers for Environmental Prediction–National Center for Atmospheric Research (NCEP–NCAR) reanalysis is used for comparison and as lateral boundary conditions for one set of regional climate experiments in this study. The NCEP–NCAR reanalysis is available at T62 spectral truncation (≈ 200 km grid resolution). In the following section the atmospheric models used in this study are discussed,

followed by a discussion on the design of experiments in section 3. In section 4 the results are presented, followed by concluding remarks in section 5.

2. Model description

The models used in this study are the Center for Ocean–Land–Atmosphere Studies (COLA) AGCM (Kinter et al. 1997) and the Regional Spectral Model (RSM; Juang and Kanamitsu 1994; Juang et al. 1997). Both models have been used extensively for seasonal climate integrations (Misra et al. 2002a,b, 2003; Misra 2004).

a. The NCEP–NCAR reanalysis and the COLA AGCM models

Owing to the nature of the anomaly nesting experiments (Misra and Kanamitsu 2004) that utilize the NCEP–NCAR reanalysis climatology and the COLA AGCM variability for lateral boundary forcing to the RSM, a brief description of the NCEP–NCAR reanalysis model is also warranted. For the sake of brevity we have outlined the features of the NCEP–NCAR reanalysis model and the COLA AGCM together in Table 1, which will also draw the reader's attention to the differences in the two models. It is apparent from the table that the two models differ considerably in their physics. Although, the PBL parameterization is from the same source, the differences in land surface, diagnostic cloud, convection and radiation schemes make its influence in the evolving climate different in the two models. The dynamical core including the orography is nearly identical except for the treatment of moisture in the two models. This yet again could make the behavior of the two models quite different from one another.

b. The RSM

The RSM initially developed by Juang and Kanamitsu (1994) and updated later in Juang et al. (1997) is

TABLE 1. The outline of the NCEP–NCAR reanalysis and the COLA AGCM models.

Feature	NCEP–NCAR reanalysis model	COLA AGCM
Dynamical core	Follows Kanamitsu et al. (1991); spectral advection of all prognostic variables; semi-implicit time integration scheme with explicit time integration for vorticity and specific humidity; mean orography	Follows Kiehl et al. (1998); spectral advection of all prognostic variables except for specific humidity, which is done by semi-Lagrangian scheme; semi-implicit time integration scheme with explicit time integration for vorticity and specific humidity; mean orography
Deep convection	Simplified Arakawa–Schubert (Pan and Wu 1995)	Relaxed Arakawa–Schubert (Moorthi and Suarez 1992)
Planetary boundary layer	Mellor and Yamada (1982); Kanamitsu (1989)	Mellor and Yamada (1982)
Longwave radiation	Fels and Schwarzkopf (1975)	Harshvardhan et al. (1987)
Shortwave radiation	Lacis and Hansen (1974)	Davies (1982)
Shallow convection	Tiedtke (1984)	Tiedtke (1984)
Land surface process	Pan and Mahrt (1987)	Xue et al. (1991, 1996)
Diagnostic cloud scheme	Campana et al. (1994)	DeWitt and Schneider (1997)
Horizontal diffusion	Leith formulation (Kanamitsu et al. 1991)	∇^4 type

used here. However, there have been changes made to the physics of this original version of the RSM, and these are outlined in Table 2. These changes include the adoption of Simplified Simple Biosphere (SSiB) model (Xue et al. 1991, 1996) detailed in Misra et al. (2002a) and the use of the relaxed Arakawa–Schubert (RAS) convection scheme when the RSM is forced with COLA AGCM at the lateral boundaries. As described in Misra et al. (2003) the regional climate integrations from the RSM over the SASM domain are sensitive at the lateral boundaries to the choice of the convection scheme between RAS and the simplified Arakawa–Schubert (SAS) scheme (Pan and Wu 1995). It is found that whenever the convection scheme used in the RSM is inconsistent with the deep convective scheme used in the global model that provides the lateral boundary conditions, large errors occur at the western boundary of the SASM domain adopted in this study.

A number of experiments are conducted that include the RSM forced at the lateral boundaries with the NCEP–NCAR reanalysis (control-A), the COLA AGCM (control-B), and a combination of the NCEP–NCAR reanalysis and the COLA AGCM (AN; Misra and Kanamitsu 2004) for this study. The RSM predicts the total field of divergence (D), vorticity (ζ), temperature (T), natural log of surface pressure ($\ln p_s$), and specific humidity (q) from which it determines the perturbations about the time-varying global field in the regional domain. These perturbations are smoothly relaxed to zero at the lateral boundaries in grid space and then Fourier transformed to satisfy solid wall boundary conditions. The RSM uses the terrain-following vertical sigma coordinate system. The model equations are integrated by a semi-implicit scheme, except the moisture and vorticity equations, which are integrated explicitly. The control-A RSM integrations have 28 σ levels identical to NCEP–NCAR reanalysis, while control-B and AN integrations of the RSM have 18 σ levels identical to that of the COLA AGCM.

For this study we have used the RSM at 80-km grid resolution with dimensions of 217×112 centered at 15°S and 80°W . The time step of the integration is 240 s. The base field is linearly interpolated in time and interpolated (using bicubic spline) in space to the RSM grid. The nesting interval for all the RSM integrations is 12 h.

TABLE 2. The outline of the physics of the original version of the RSM (Juang et al. 1997).

Physical process	Scheme
Deep convection	Pan and Wu (1995)
Shortwave radiation	Chou (1992)
Longwave radiation	Fels and Schwarzkopf (1975)
Boundary layer	Miyakoda and Sirutis (1977)
Vertical diffusion	Hong and Pan (1996)
Shallow convection	Tiedtke (1984)
Gravity wave drag	Alpert et al. (1988)
Cloud radiation interaction	Slingo (1987)
Land surface process	Pan and Mahrt (1987)

3. Design of experiments

For this study we have used model runs from past studies (Misra et al. 2002a, 2003; Misra and Kanamitsu 2004). A brief outline of these experiments is given in Table 3. The COLA AGCM, control-B, and AN experiments all had a start date of 0000 UTC 15 December of 1996, 1997, and 1998 for all five ensemble members. Control-A had a start date of 0000 UTC 13 December for the same years as the rest of the experiments, and it used the NCEP–NCAR reanalysis interpolated to the RSM grid for its atmospheric initial conditions. The atmospheric initial conditions of control-B, COLA-AGCM, and AN experiments are identical and are described in Misra et al. (2003). All these model integrations were carried out for a period of three-and-a-half months to the end of March of the following year. In the case of AN experiments, for each member of the ensemble of the COLA AGCM, its climatology computed from several hindcast seasonal integrations is removed and replaced with the corresponding climatology of the NCEP–NCAR reanalysis (Misra and Kanamitsu 2004). In all the model integrations of this study the surface boundary condition of SST is obtained from the weekly blended SST of Reynolds and Smith (1994), and soil moisture fields are initialized from a 2-yr climatology of the Global Soil Wetness Project (Dirmeyer and Zeng 1999). The snow cover in the COLA AGCM was initialized from seasonally varying climatological data that are derived from seasonal albedo data.

4. Results

For observational verification and analysis we use OLR following Liebmann and Smith (1996) obtained from the Web site of the National Oceanic and Atmospheric Administration–Cooperative Institute for Research in the Environmental Sciences (NOAA–CIRES) Climate Diagnostics Center, Boulder, Colorado (<http://www.cdc.noaa.gov>). This is available daily at 2.5° resolution from 1974 to the present. As stated earlier, we are examining the intraseasonal anomalies from the model and observations in reference to OLR only. There are essentially two kinds of variances that are computed, namely, ensemble mean variance (EMV; described in appendix a) and variance of the ensemble mean (VEM; described in appendix b). The presence of VEM signifies that the variance is predictable since it is forced by the slowly varying surface and/or lateral boundary conditions. On the other hand, EMV refers to average variance, which contains both the model noise and the signal components. The OLR from both the observations and the model output are passed through the first-order Butterworth (1930) filter to obtain anomalies at the 20–40-day time scale for January–February–March (JFM) of 1997, 1998, and 1999. This filter is a linear bandpass recursive filter, which has been adopted in the past for such studies (Murakami

TABLE 3. The details of the experiments conducted in this study. LBC stands for lateral boundary conditions.

Name of Experiment	Model used	Domain	LBC forcing	No. of ensemble members	Reference
COLA AGCM	COLA AGCM	Global	—	5	Misra et al. (2003)
Control-A	RSM	Regional	NCEP–NCAR reanalysis	—	Misra et al. (2002a)
Control-B	RSM	Regional	COLA AGCM NCEP–NCAR reanalysis climatology	5	Misra et al. (2003)
AN	RSM	Regional	and COLA AGCM anomalies	5	Misra and Kanamitsu (2004)

1979; Krishnamurti and Subrahmanyam 1982). In the ensuing subsection the observations are analyzed, followed by the comparison of the NCEP–NCAR reanalysis and COLA AGCM. In the following subsections the results from the control-A, control-B, and AN integrations of the RSM are discussed.

a. Observations

In Fig. 1 the mean seasonal (JFM) variance of the observed OLR is shown at intraseasonal scales for 1997, 1998, and 1999. It is clearly seen that the variance is relatively large over the SACZ, the Brazilian highlands, and Paraguay, and over the northwestern part of South America, which is consistent with other observational studies (Liebmann et al. 1999). There is also a region of large variance over the South Pacific Ocean evident in all 3 yr. Kousky and Kayano (1994) and Grimm and Silva Dias (1995) indicate that the modulation of the convection in the SPCZ region by the MJO can influence the variability of the SACZ at intraseasonal scales. Liebmann et al. (1999) show that the region over Paraguay south of the Amazon River basin (ARB) has a minimum of interannual variance that in fact extends from the ARB, indicating that subseasonal variability constitutes an important source of variability in the region. Velasco and Fritsch (1987) and Mohr and Zipser (1996) show in their observational study that this region of large subseasonal variability coincides with a region of most frequent mesoscale convective complexes. In another related study, Jones and Carvalho (2002) show that the wet and dry spells of the SASM have distinct associated low-level circulation anomalies. They show from NCEP–NCAR reanalysis that wet (dry) spells over the Brazilian highlands relate to westerly (easterly) flow regime over the region. They also indicate that over northwestern Brazil and Venezuela, the OLR anomalies reverse sign from westerly to easterly regimes.

The three seasons of JFM 1997, 1998, and 1999 are representative of neutral, warm, and cold ENSO events (Misra et al. 2002b), respectively. A similar interannual variability is also clearly seen in the intraseasonal variance of the OLR over the EEPO and eastern Brazil. In 1998, the intraseasonal variance of OLR over the EEPO (eastern Brazil and South Atlantic convergence zone) is relatively large (small) compared to 1997 and 1999.

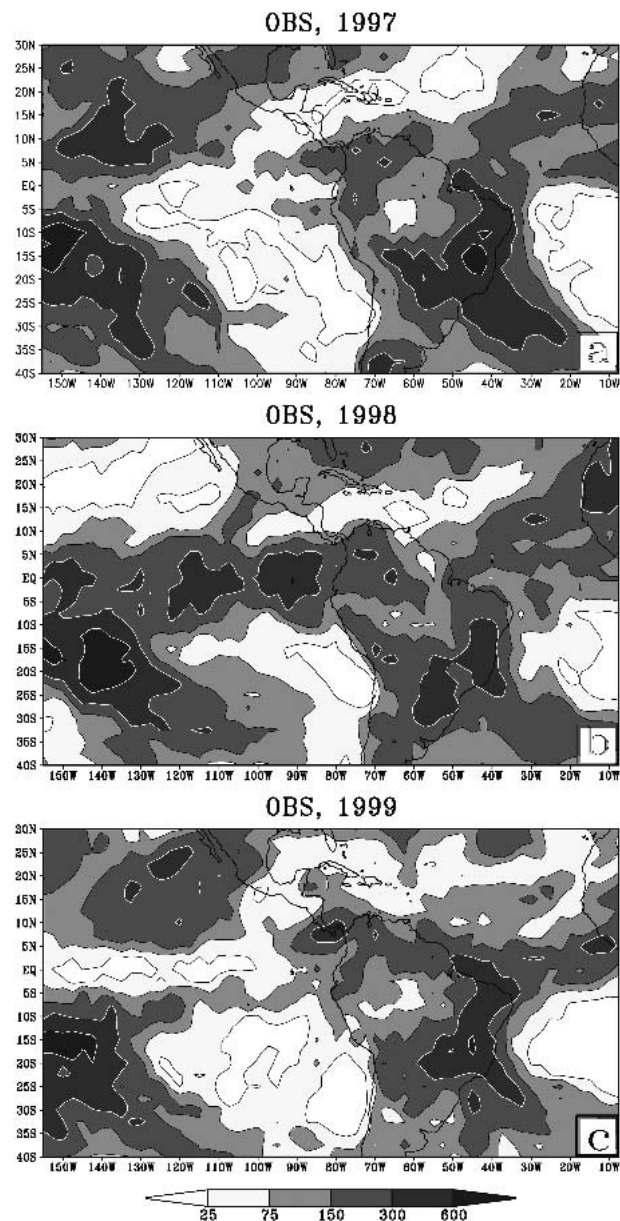


FIG. 1. The observed (Liebmann and Smith 1996) variance-filtered OLR anomalies at a 20–40-day time scale for JFM of (a) 1997, (b) 1998, and (c) 1999. The units are in $W^2 m^{-4}$. Contours over $300 W^2 m^{-4}$ are drawn in white for clarity.

b. NCEP–NCAR reanalysis and COLA AGCM

In Fig. 2 the mean JFM intraseasonal variance of OLR from the NCEP–NCAR reanalysis and COLA AGCM are presented for 1997, 1998, and 1999. It should be noted here that in the case of COLA AGCM we have plotted EMV. In comparison to Fig. 1 both the NCEP–NCAR reanalysis and COLA AGCM show weaker variance than observed over the whole regional domain. The (coarse) horizontal resolution of the NCEP–NCAR reanalysis and COLA AGCM are able to capture some, albeit weak, intraseasonal variance over the South Pacific Ocean, the SACZ region, and the Brazilian highlands. The interannual variability of the intraseasonal variance over the EEPO and eastern Brazil is weak to nonexistent in both the COLA AGCM and the NCEP–NCAR reanalysis. However, the NCEP–NCAR reanalysis (COLA AGCM) does exhibit, albeit weakly, some interannual variability of the intraseasonal variance over the SPCZ (EEPO) region.

c. Regional climate integrations

Similar to Fig. 2 the mean JFM intraseasonal variance (EMV) of OLR from control-A and control-B integrations of the RSM is shown in Fig. 3. It is apparent from Fig. 3 that the control-A integrations are able to simulate the intraseasonal variance more realistically than the control-B integrations. The variance over the South Pacific, the SACZ region, the Brazilian highlands, and the northwestern part of South America compare well with observations and indicate appreciable improvement from NCEP–NCAR reanalysis. However, downscaling the COLA AGCM integrations (by nearly a factor of 4 in terms of horizontal resolution) in the control-B run produced no improvement. In fact, over the EEPO region, the variance in the control-B run decreased further (Fig. 3e) from the already weak variance displayed by the COLA AGCM (Fig. 2e).

The control-A integrations show an improved interannual variability of the intraseasonal variance over the

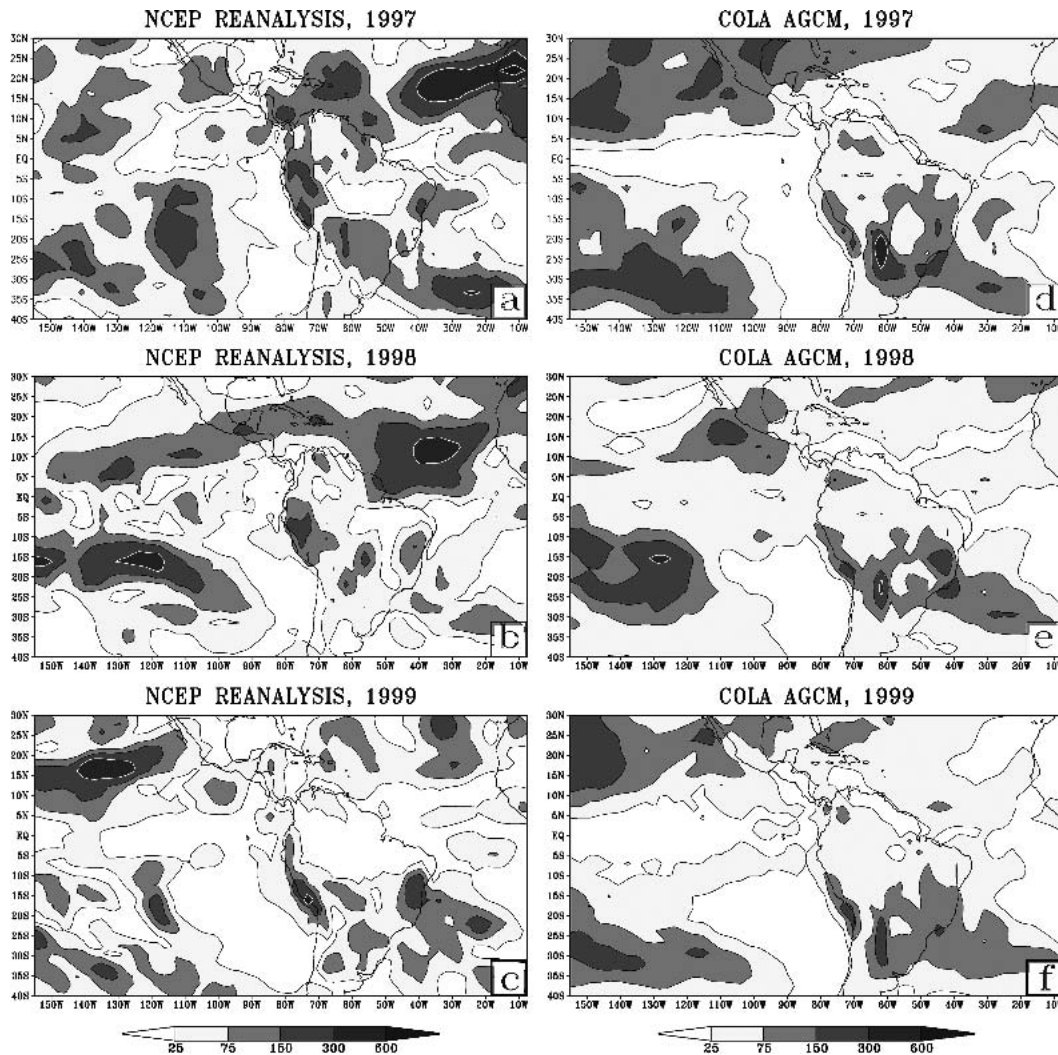


FIG. 2. Same as Fig. 2, but from NCEP–NCAR reanalysis and COLA AGCM.

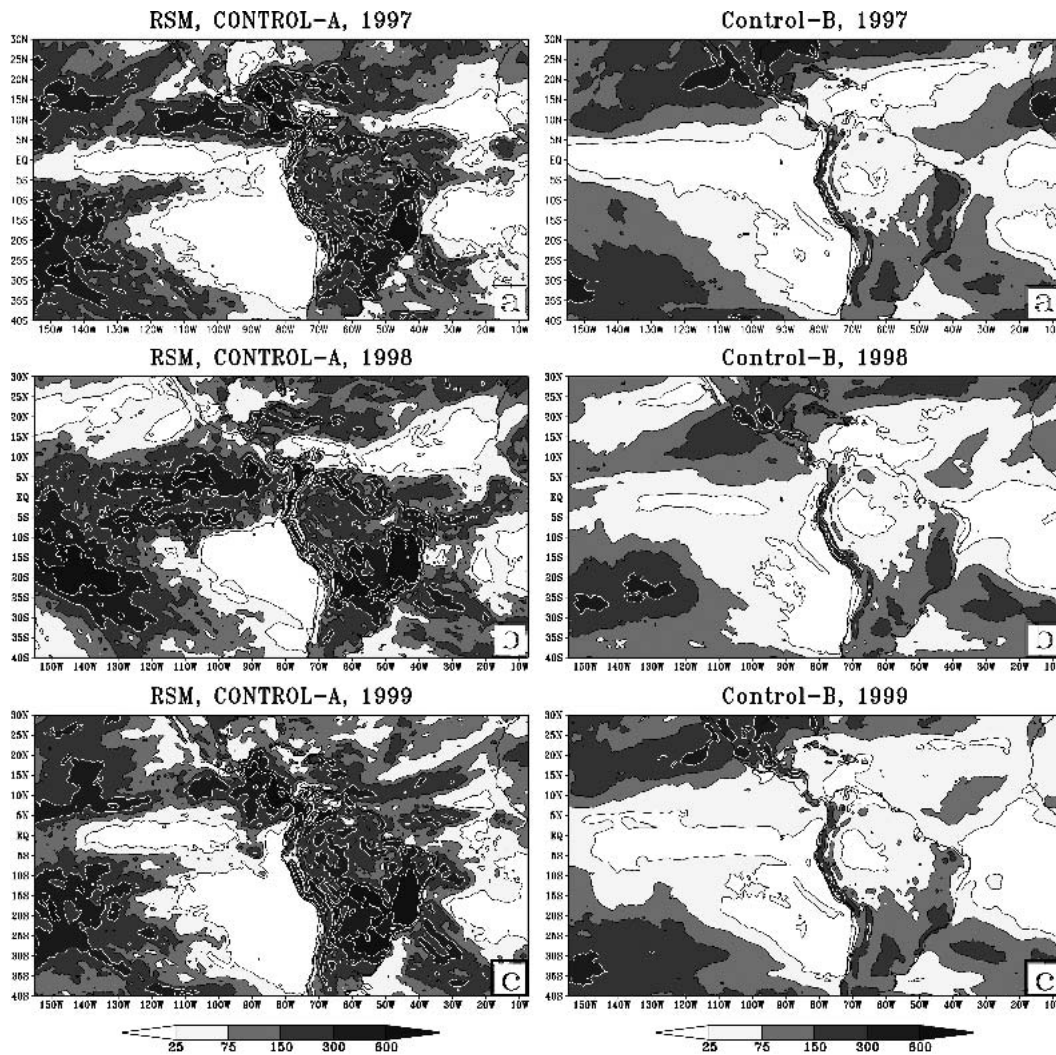


FIG. 3. Same as Fig. 2, but from control-A and control-B RSM integrations.

EEPO region, along eastern Brazil, and over Paraguay. However, control-B runs indicate extremely weak to nonexistent interannual variability over these regions. The results from control-A seem to suggest that the intraseasonal variance of OLR is weaker over Paraguay and the Brazilian highlands during warm ENSO events (JFM 1998) relative to cold ENSO events (JFM 1999). This is also seen in observations from the composite difference of intraseasonal variance of OLR between three warm and cold ENSO events (not shown). The larger variance over the EEPO region in 1998 relative to 1997 and 1999 displayed by control-A is also in agreement with observations over Brazil (see Fig. 1).

The mean JFM intraseasonal variance from the anomaly nesting procedure (Misra and Kanamitsu 2004) is shown in Fig. 4. The premise of the AN run is that the evolving regional climate in the RSM avoids the climate drift imposed at the lateral boundary conditions from the COLA AGCM. Misra (2004) showed

that the COLA AGCM exhibits large climate drift over South America and the surrounding oceans. It is seen from Fig. 4 that the mean intraseasonal variance over the Brazilian highlands and Paraguay in the AN integration is considerably improved compared to the control-B run. Furthermore, the variance displayed over the SACZ and the EEPO also compare reasonably well with observations. The AN integrations capture the interannual variation of the intraseasonal variance over the EEPO region. But over eastern Brazil the variability is weak relative to the control-A integration. Furthermore, the AN integrations generally display larger variance than the observations in all seasons over most parts of the regional domain. These deficiencies in the AN runs, which are not present in control-A integrations, point to errors propagating from the lateral boundary conditions through the anomalies of the COLA AGCM. The larger-than-observed variance exhibited in Fig. 4, especially along the western boundary

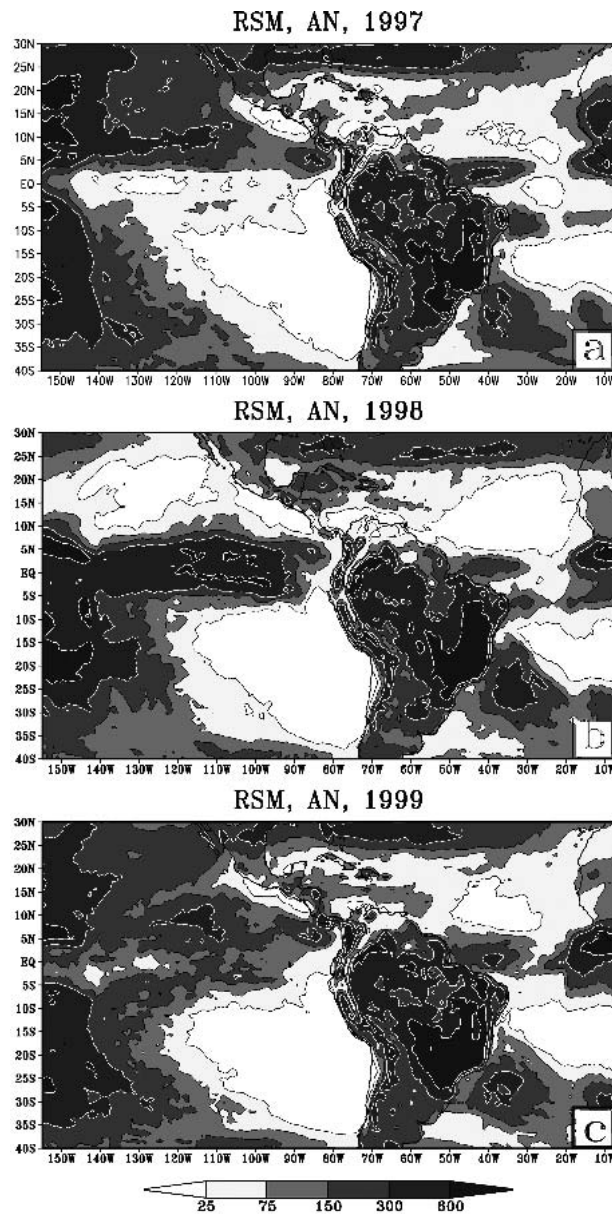


FIG. 4. Same as Fig. 2, but from AN RSM integration.

of the regional domain, is a result of the incompatibility of the convection schemes of the NCEP–NCAR reanalysis assimilation model, which uses the SAS scheme (Pan and Wu 1995), and the COLA AGCM, which uses the RAS scheme. A similar feature is also observed in the eastern boundary over western Africa.

In summary, the AN integrations demonstrate that the systematic errors of the COLA AGCM suppress the intraseasonal variability in the control-B integrations.

d. Diurnal variation

It is important to understand the cause of the differences in these model results to comprehend the simu-

lation of the intraseasonal variability of the SASM. In this subsection we explore one potential cause of this difference, namely, diurnal variability of OLR. Garreaud and Wallace (1997), using infrared data from geostationary satellites, found that convective cloudiness shows a prominent diurnal cycle, especially along a band over the Andes Mountains in the northeast coast of South America and in two intermediate parallel bands over Amazonia. They further show from their analysis that the diurnal cycle is coherent over the land areas with relatively clear mornings and a more gradual nighttime decay. Yang and Slingo (2001), using an archive of global distribution of brightness temperatures, showed similar diurnal cycle features over South America. In a related idealized modeling study over South America, Figueroa et al. (1995) show that the diurnal variation of convection over the ARB is critical for the maintenance of the SACZ region.

In Figs. 5 and 6 the mean JFM variance of OLR at intraseasonal scales from control-A and control-B integrations at 6-h intervals is shown using the OLR fields saved at 0000, 0006, 0012, and 0018 UTC for 1998, respectively. For brevity, the figures for 1998 only are shown, as they are similar for 1997 and 1999. It is apparent from Fig. 5 that control-A has a strong diurnal variation in the intraseasonal activity over the Brazilian highlands and Paraguay, peaking in the late afternoon (0018 UTC) and evening (0000 UTC) and decaying at night (0006 UTC) and in the early morning (0012 UTC). This diurnal march of the intraseasonal variance is similar to the observed diurnal march indicated in Yang and Slingo (2001) and Betts (2002). However, control-B shows a much weaker diurnal variation and is almost 180° out of phase relative to control-A. Furthermore in control-A (Fig. 5) a weak semidiurnal cycle in the intraseasonal variance is observed over the oceans, especially over the equatorial Pacific Ocean, with OLR intraseasonal variance peaking at 0000 and 1200 UTC and reaching a nadir at 0006 and 0018 UTC. Control-B runs do not indicate any such semidiurnal variability over the oceans.

In Fig. 7 we have similarly plotted the diurnal march of the mean JFM intraseasonal variance of OLR for 1998 from the AN runs. Figure 7 shows similar features to that of the control-A integrations such as the robust diurnal cycle over the Paraguay region, the Brazilian highlands, the SACZ region, the northwestern part of South America, and the relatively weak semidiurnal variation over the Pacific Ocean. In fact, the diurnal amplitude of the intraseasonal variance of OLR is higher in the AN run relative to the control-A run over most areas in the domain.

The results from control-A and AN runs suggest that diurnal (semidiurnal) variability of the intraseasonal variance over land (ocean) is an important component of intraseasonal variability of the SASM and the EEPO. It should be mentioned that unfiltered OLR in control-A and AN runs showed an evolution of the

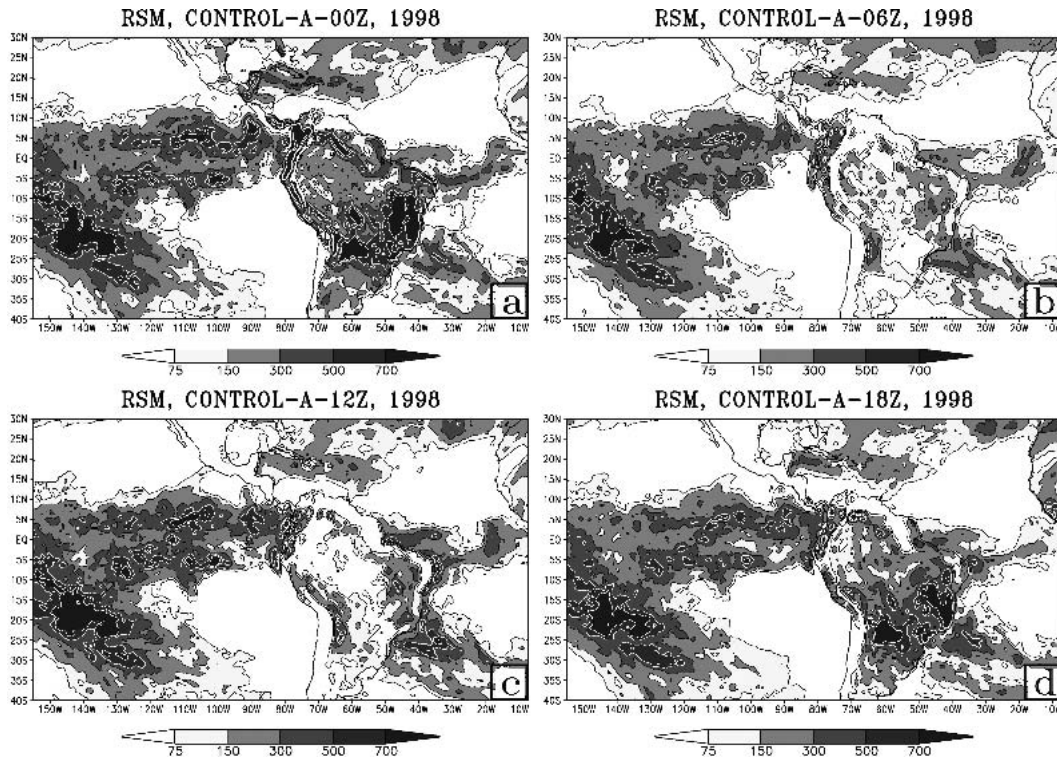


FIG. 5. Same as Fig. 2, but using OLR values valid at (a) 0000, (b) 0006, (c) 0012, and (d) 0018 UTC from control-A integrations.

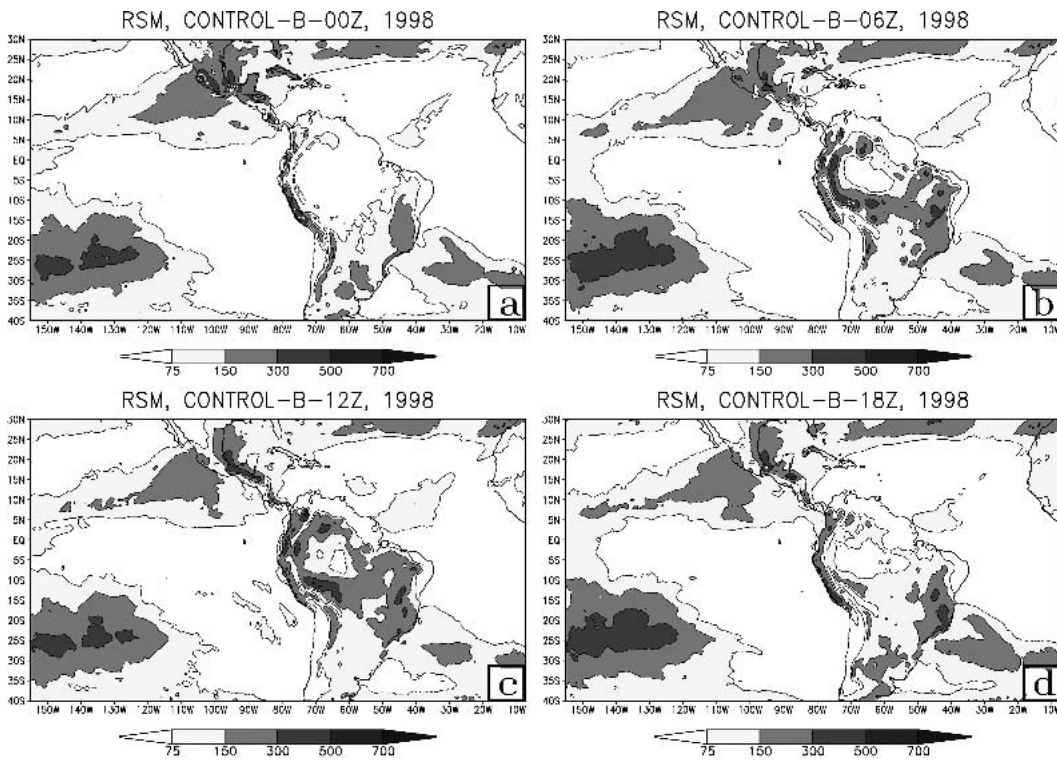


FIG. 6. Same as Fig. 5, but from control-B integrations.

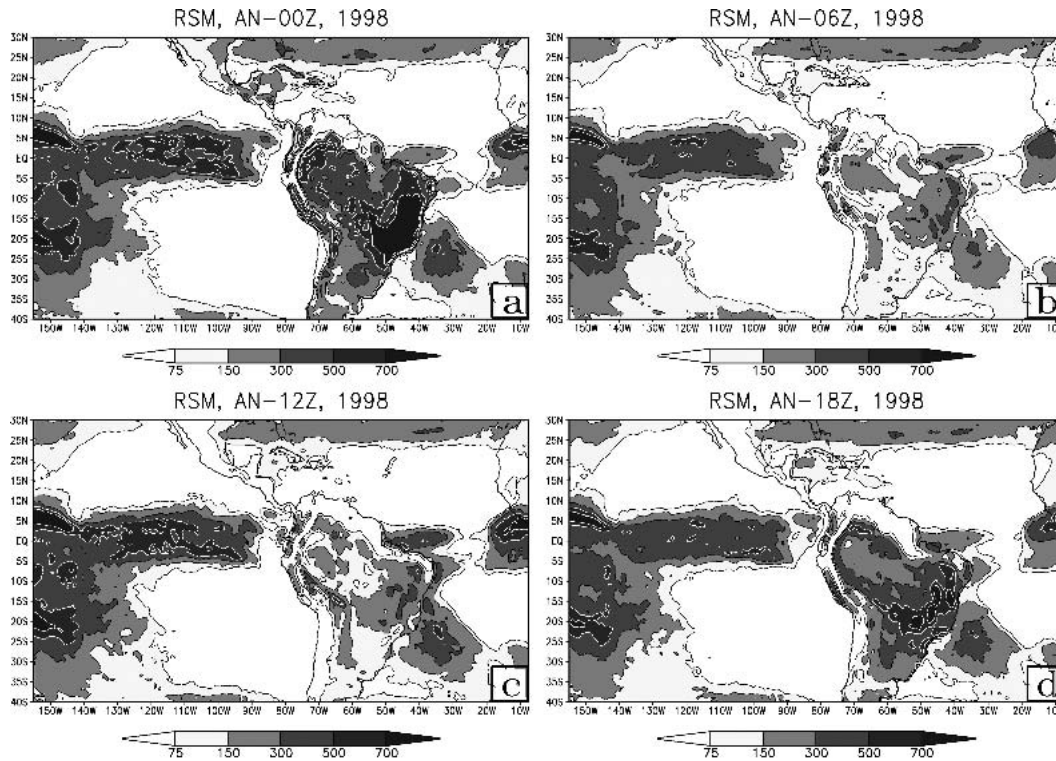


FIG. 7. Same as Fig. 5, but from AN integrations.

diurnal and semidiurnal cycle (not shown) similar to the intraseasonal variance of OLR. In control-B, the diurnal (semidiurnal) cycle of the unfiltered OLR was weak (nonexistent) and 180° out of phase relative to the AN and control-A runs.

e. Potential predictability of intraseasonal variability

Here we will be examining the predictability of intraseasonal anomalies from the AN runs as they are the most promising of all the model potential prediction runs in this study. Although the control-A integrations also show reasonable intraseasonal variance, it should be remembered that the RSM in control-A is forced with NCEP–NCAR reanalysis at the lateral boundary conditions, which relegates it to a simulation rather than a potential prediction run. “Potential” predictability is referred to in conjunction with the AN runs as that is the upper limit of the skill that can be attained if predicted SST is used instead of the observed SST as the surface boundary conditions over the oceans.

Plotted in Fig. 8 is the mean JFM signal-to-noise (STN; see appendix B) ratio of the intraseasonal variance computed from the daily mean OLR for 1997, 1998, and 1999. In the figure we have masked out the STN ratio in areas where the intraseasonal OLR anomalies are below 5 W m^{-2} . In the figure, a ratio of

1 indicates that intraseasonal variance is fully predictable, while 0 would relate to model noise. It is seen from the figure that there is comparatively little predictability over the Brazilian highlands and Paraguay and also over the EEPO region.

Similarly, the mean JFM STN ratio is plotted for 0000, 0006, 0012, and 0018 UTC for 1998 in Fig. 9. This figure shows predictability over land peaks at 1200 UTC and gradually decays to a minimum at 0000 UTC. This is in stark contrast to the diurnal march of the intraseasonal variance observed in Fig. 7, which peaks at 0000 UTC and reaches a minimum at 1200 UTC. In the other two years (1997 and 1999) similar behavior is observed (not shown). Over the oceans, a semidiurnal cycle of the STN ratio is observed, especially over the South Pacific Ocean, showing relatively large values of the ratio at 0006 and 0018 UTC, in contrast to the peak in variance observed at 0000 and 0012 UTC. Therefore it is apparent from this discussion that the large intraseasonal variance over the EEPO, Brazilian highlands, and Paraguay are largely generated from the model’s internal variability. This indicates that deterministic seasonal prediction of intraseasonal variability of the SASM and over the EEPO is rather difficult.

In Fig. 10, similar to Fig. 9, the STN ratio for the diurnal variance of OLR is plotted. This figure clearly shows that the wet phase of the diurnal cycle that peaks at 0000 UTC over the Amazon, Brazilian highlands,

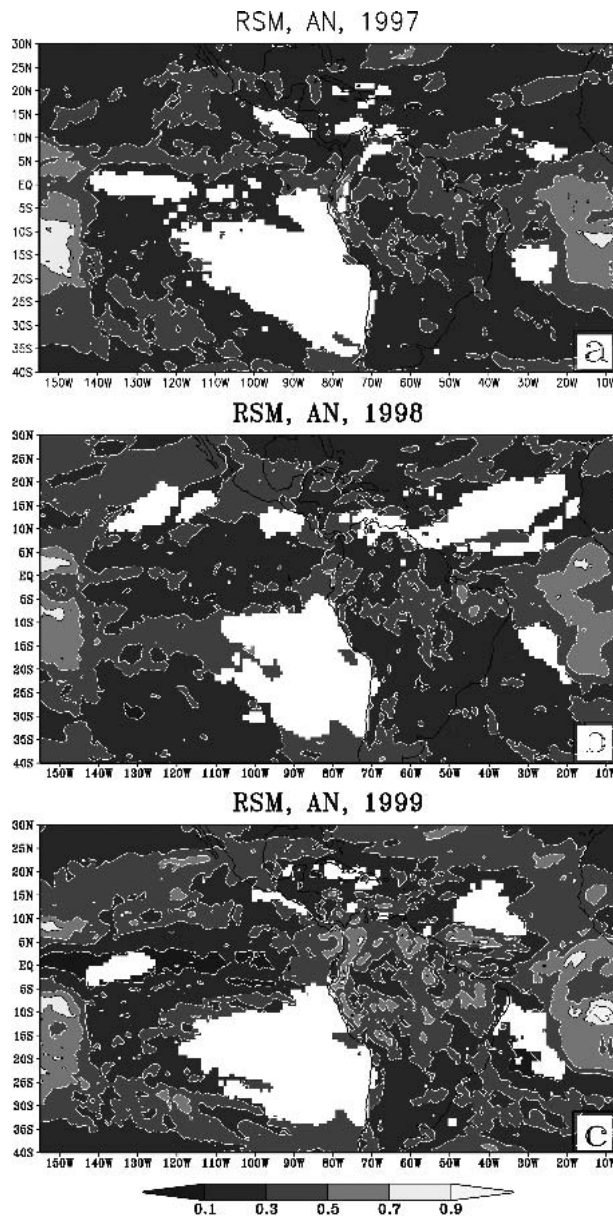


FIG. 8. The mean JFM STN ratio computed from the daily mean OLR derived from the AN experiment. The STN ratio is masked in regions where the daily mean OLR values are lower than 5 W m^{-2} . The contours over 0.7 are drawn in black for clarity.

and Paraguay is far more predictable (reproducible by the ensemble members of the AN runs) than the dry phase. The AN methodology shows that the diurnal variation of the intraseasonal variance over the region is a feature of the region that is different from the externally forced diurnal variation. The AN runs demonstrate that the diurnal rectification imposed by the NCEP–NCAR climatology at the lateral boundaries of the RSM ameliorates the systematic errors of the COLA AGCM (Misra and Kanamitsu 2004), thereby producing verifiable intraseasonal variability.

5. Summary and conclusions

This study was motivated from the success of the anomaly nesting in simulating the intraseasonal variability of OLR (Misra and Kanamitsu 2004). The observational studies of Paegle and Mo (1997), Liebmann et al. (1999), and Jones and Carvalho (2002) have identified the SACZ, Brazilian highlands, northwestern Brazil, and the Paraguay region as having robust intraseasonal variability during the SASM period. In this study it is shown that the coarse-resolution NCEP–NCAR reanalysis ($\approx 200 \text{ km}$) and COLA AGCM ($\approx 300 \text{ km}$) significantly underestimate the intraseasonal variance of the SASM. However, a substantial benefit is realized when the NCEP–NCAR reanalysis is downscaled using RSM to 80-km resolution (control-A experiment). The variance over the Brazilian highlands, SACZ, Paraguay, SPCZ, and over the EEPO is nearly restored. It should be noted that past studies (Kiladis and Weickmann 1992; Grimm and Silva Dias 1995) have shown that the modulation of SPCZ related to the MJO can modulate the SACZ convection at intraseasonal scales through Rossby wave propagation. Therefore, the improvement seen over the South Pacific Ocean has significance to the improvement seen in the SACZ region in the control-A experiment. However, downscaling the COLA AGCM seasonal integration using RSM (control-B experiment) did not yield the same encouraging results as control-A. The anomaly nesting (AN) experiment produced reasonable results relative to control-B. In most areas the intraseasonal variance of AN was higher than that in control-A. But unlike control-B, AN experiments displayed a distinct region of large intraseasonal variance over the Brazilian highlands, Paraguay, northwestern Brazil, SACZ, SPCZ, and EEPO regions.

It was found, in further analyzing the results to determine the cause of the difference in these model runs, that the intraseasonal variance had a large (relatively smaller) diurnal (semidiurnal) component over land (ocean) with nearly identical phase between control-A and AN experiments. In addition, it was found that this diurnal cycle of the intraseasonal variance was similar to the observed diurnal changes in brightness temperatures (Yang and Slingo 2001). The control-B runs show a much smaller diurnal cycle of the intraseasonal variance of OLR over land, barely any semblance of semidiurnal cycle over oceans, and a phase nearly opposite to that of control-A and AN experiments.

We also examined the signal-to-noise (STN) ratio of the intraseasonal variability of OLR from the AN experiment. AN was the only set of prediction experiments that showed promising results at intraseasonal scales. This analysis showed that the intraseasonal variability arises from the internal variability of the nonlinear dynamical model. This result is not very surprising as Krishnamurti et al. (2003) showed that disturbances at intraseasonal time scales can substantially be ampli-

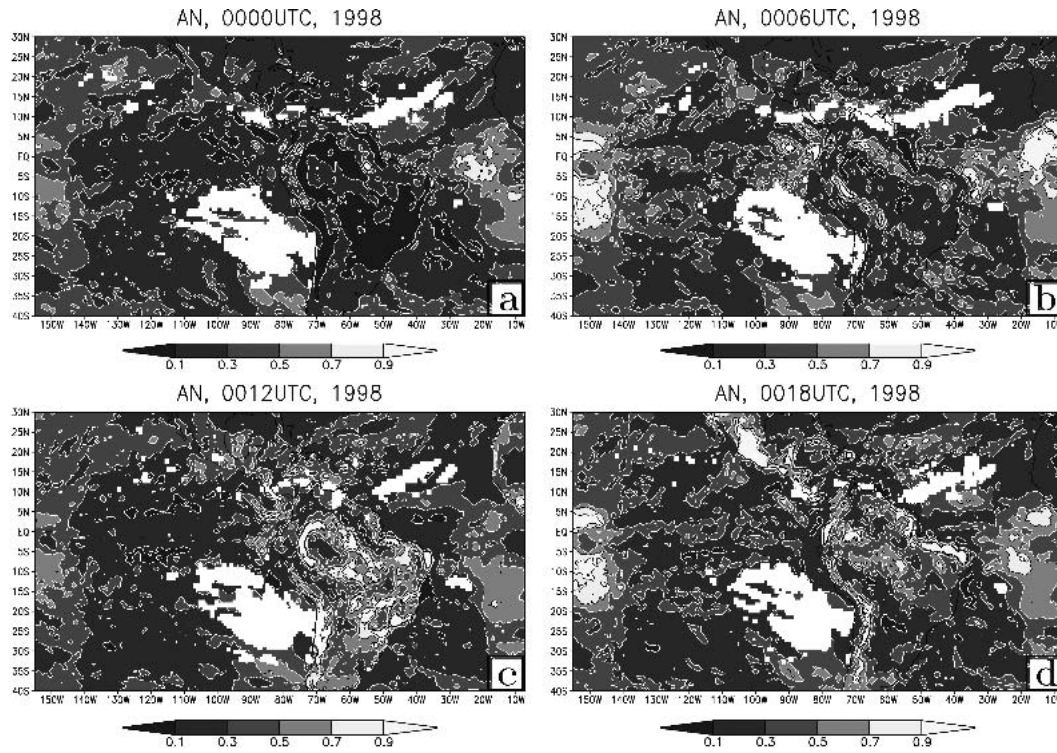


FIG. 9. Same as Fig. 8 but using OLR valid at (a) 0000, (b) 0006, (c) 0012, and (d) 0018 UTC.

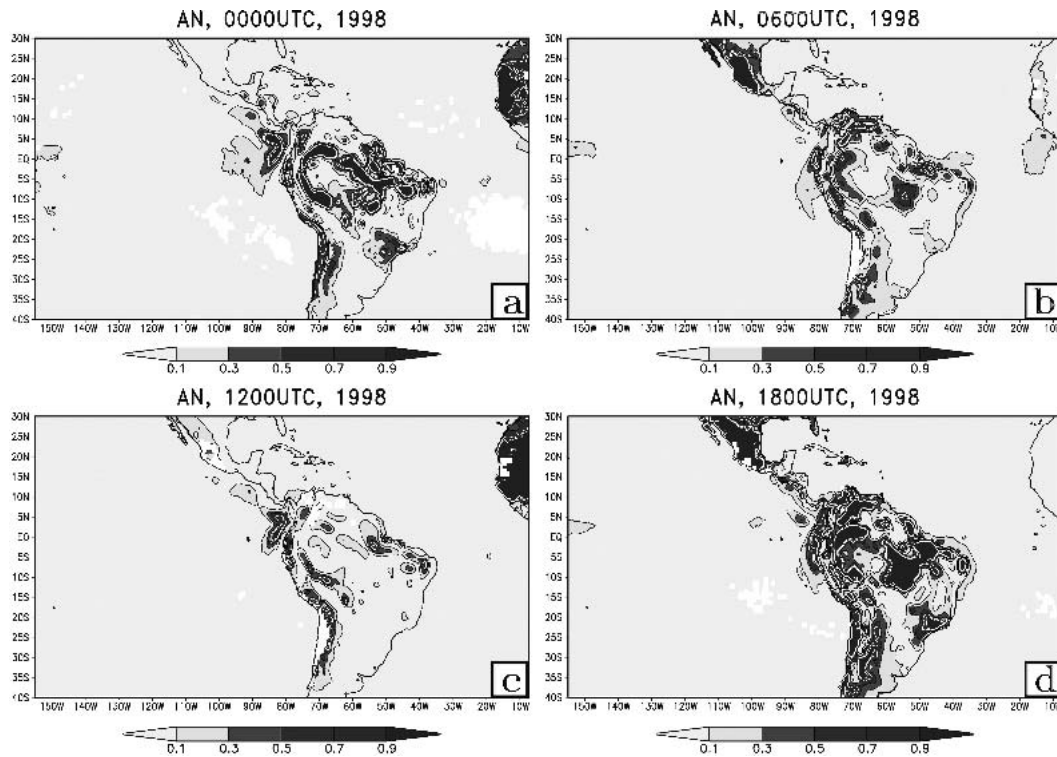


FIG. 10. The mean JFM STN ratio for variance of OLR at diurnal scales from the AN experiment at (a) 0000, (b) 0600, (c) 1200, and (d) 1800 UTC. The STN ratio is masked in regions where the diurnal anomalies are less than 5 W m^{-2} . The contours over 0.7 are drawn in white for clarity.

fied from nonlinear-scale interactions at synoptic scales. In other words, weather (noise) can modulate intraseasonal variability. Furthermore, there is a growing consensus in the community that intraseasonal oscillation is a coupled ocean-atmosphere phenomenon (Zheng et al. 2003; Jones and Weare 1996). Although this theory cannot be tested rigorously in the modeling framework of this study, it is evident that even over open oceans in the eastern Pacific under warm ENSO conditions (1998), the control-B integrations showed extremely weak intraseasonal activity. The AN run with largely a diurnal rectification to the large-scale atmospheric conditions in the control-B run was able to retrieve most of the observed intraseasonal variance in the regional domain including that over the eastern Pacific Ocean, suggesting that the intraseasonal variability over the South American region and the neighboring ocean basins may be a result of the internal variability of the coupled ocean-land-atmosphere process.

This study showed that there is a distinct diurnal cycle of the STN ratio that is nearly opposite in phase to the diurnal cycle of the intraseasonal variance. Alternatively, the predictability is found to be largest (smallest) when the diurnal cycle of the intraseasonal variance reaches its nadir (zenith). Similarly, over the oceans, especially over the South Pacific Ocean, predictability was found to be opposite in phase to the semidiurnal cycle of the intraseasonal variance. One could conclude then that the systematic errors of the COLA AGCM, communicated from the lateral boundary, erroneously suppress the generation of the intraseasonal variability in the RSM. In contrast to the STN ratio of the intraseasonal variability, the diurnal scales in the AN runs show larger predictability when the diurnal variance reaches its zenith. This further shows that the AN runs distinguish the physical processes involved in the diurnal and intraseasonal variability. The diurnal variation of the intraseasonal variance is a feature of the subseasonal variance over the region.

This study clearly demonstrates that downscaling coarse-resolution analysis or coarse AGCM integrations with a realistic diurnal cycle is beneficial at intraseasonal scales. This study also points to a certain interaction between the diurnal (semidiurnal) cycle and the intraseasonal scales of OLR, which is critical for simulating the intraseasonal variance over the Brazilian highlands, neighboring Paraguay region, and over the EEPO. The dynamics of this interaction has to be addressed via detailed energy budget studies using analysis in the wavenumber and frequency domain, an endeavor that is beyond the scope of this paper. A rather disappointing result of this study is that the intraseasonal variability in the AN integration arises mostly from the model's internal variability, which precludes us from investigating the evolution of these anomalies from an ensemble of seasonal model integrations.

Acknowledgments. The author acknowledges the useful suggestions made by Drs. David Straus and Ben Kirtman while preparing this manuscript. The author also acknowledges the useful comments made by two anonymous reviewers that greatly improved the overall quality of the paper. This study was supported by NSF Grant ATM9814295, NASA Grant NAG5-11656, and NOAA Grant NA16GP2248. The interpolated OLR data were provided by the NOAA-CIRES Climate Diagnostics Center, Boulder, Colorado, from their Web site at <http://www.cdc.noaa.gov/>.

APPENDIX A

Ensemble Mean Variance (EMV)

$$\text{EMV} = \frac{1}{M} \sum_{j=1}^M (\text{EMV}_j), \quad (\text{A1})$$

where

$$\text{EMV}_j = \frac{1}{N-1} \sum_{i=1}^N (x_{ij})^2, \quad (\text{A2})$$

where x_{ij} is the filtered OLR on the i th day of the season of the j th ensemble member, N is the total number of days in the season, and M refers to the total number of ensemble members.

APPENDIX B

Variance of the Ensemble Mean (VEM)

$$\text{VEM} = \frac{1}{N-1} \sum_{i=1}^N (X_i)^2, \quad (\text{B1})$$

where X_i is the ensemble mean of filtered OLR for the i th day:

$$X_i = \frac{1}{M} \sum_{j=1}^M (x_{ij}). \quad (\text{B2})$$

Then the STN ratio is given by

$$\text{STN} = \frac{\text{VEM}}{\text{EMV}}. \quad (\text{B3})$$

When STN is equal to 0 (1) then it signifies model noise (signal).

REFERENCES

- Alpert, J. C., M. Kanamitsu, P. M. Caplan, J. G. Sela, G. H. White, and E. Kalnay, 1988: Mountain induced gravity wave drag parameterization in the NMC medium-range forecast model. Preprints, *Eighth Conf. on Numerical Weather Prediction*, Baltimore, MD, Amer. Meteor. Soc., 726-733.
- Betts, A. K., and C. Jakob, 2002: Evaluation of the diurnal cycle of precipitation, surface thermodynamics, and surface fluxes in the ECMWF model using LBA data. *J. Geophys. Res.*, **107**, 8045, doi:10.1029/2001JD000427.

- Butterworth, S., 1930: On the theory of filter amplifiers. *Exp. Wireless Radio Eng.*, **7**, 536–541.
- Campana, K. A., Y.-T. Hou, K. E. Mitchell, S.-K. Yang, and R. Cullather, 1994: Improved diagnostic cloud parameterization in NMC's global model. Preprints, *10th Conf. on Numerical Weather Prediction*, Portland, OR, Amer. Meteor. Soc., 324–325.
- Chou, M.-D., 1992: A solar radiation model for use in climate studies. *J. Atmos. Sci.*, **49**, 762–772.
- Davies, R., 1982: Documentation of the solar radiation parameterization in the GLAS climate model. NASA Tech. Memo. 83961, 57 pp.
- DeWitt, D. G., and E. K. Schneider, 1997: The earth radiation budget as simulated by the COLA GCM. COLA Rep. 35, 39 pp. [Available from COLA, 4041 Powder Mill Rd., Suite 302, Calverton, MD 20705.]
- Dirmeyer, P. A., and F. J. Zeng, 1999: An update to the distribution and treatment of vegetation and soil properties in SSiB. COLA Tech. Rep. 78, 25 pp. [Available from Center for Ocean–Land–Atmosphere Studies, 4041 Powder Mill Road, Suite 302, Calverton, MD 20705.]
- Fels, S. B., and M. D. Schwarzkopf, 1975: The simplified exchange approximation: A new method for radiative transfer calculations. *J. Atmos. Sci.*, **32**, 1475–1488.
- Figueroa, S. N., P. Satyamurty, and P. L. da Silva Dias, 1995: Simulations of the summer circulation over the South American region with an eta coordinate model. *J. Atmos. Sci.*, **52**, 1573–1584.
- Garreaud, R. D., and J. M. Wallace, 1997: The diurnal march of convective cloudiness over the Americas. *Mon. Wea. Rev.*, **125**, 3157–3171.
- Grimm, A. M., and P. L. Silva Dias, 1995: Analysis of tropical–extratropical interactions with influence functions of a barotropic model. *J. Atmos. Sci.*, **52**, 3538–3555.
- Harshvardhan, R. Davies, D. A. Randall, and T. G. Corsetti, 1987: A fast radiation parameterization for atmospheric circulation models. *J. Geophys. Res.*, **92** (D1), 1009–1016.
- Hendon, H. H., and B. Liebmann, 1990: The intraseasonal (40–50 day) oscillation of the Australian summer monsoon. *J. Atmos. Sci.*, **47**, 2227–2240.
- Hong, S.-Y., and H.-L. Pan, 1996: Nonlocal boundary layer vertical diffusion in a medium-range forecast model. *Mon. Wea. Rev.*, **124**, 2322–2339.
- Jones, C., and B. C. Weare, 1996: The role of low-level moisture convergence and ocean latent heat fluxes in the Madden and Julian oscillation: An observational analysis using ISCCP data and ECMWF analyses. *J. Climate*, **9**, 3086–3104.
- , and L. M. V. Carvalho, 2002: Active and break phases in the South American monsoon system. *J. Climate*, **15**, 905–914.
- Juang, H.-M. H., and M. Kanamitsu, 1994: The NMC nested regional spectral model. *Mon. Wea. Rev.*, **122**, 3–26.
- , S.-Y. Hong, and M. Kanamitsu, 1997: The NCEP regional spectral model: An update. *Bull. Amer. Meteor. Soc.*, **78**, 2125–2143.
- Kanamitsu, M., 1989: Description of the NMC Global Data Assimilation and Forecast System. *Wea. Forecasting*, **4**, 335–342.
- , and Coauthors, 1991: Recent changes implemented into the global forecast system at NMC. *Wea. Forecasting*, **6**, 425–435.
- Kessler, W. S., and R. Kleeman, 2000: Rectification of the Madden–Julian oscillation into the ENSO cycle. *J. Climate*, **13**, 3560–3575.
- Kiehl, J. T., J. J. Hack, G. Bonan, B. A. Boville, D. L. Williamson, and P. J. Rasch, 1998: The National Center for Atmospheric Research Community Climate Model: CCM3. *J. Climate*, **11**, 1131–1149.
- Kiladis, G. N., and K. M. Weickmann, 1992: Circulation anomalies associated with tropical convection during northern winter. *Mon. Wea. Rev.*, **120**, 1900–1923.
- Kinter, J. L., III, and Coauthors, 1997: The COLA Atmosphere–Biosphere General Circulation Model. Volume 1: Formulation. COLA Tech. Rep. 51, 44 pp. [Available from COLA, 4041 Powder Mill Road, Suite 302, Calverton, MD 20705.]
- Kousky, V. E., and M. T. Kayano, 1994: Principal modes of outgoing longwave radiation and 250-mb circulation for the South American sector. *J. Climate*, **7**, 1131–1143.
- Krishnamurti, T. N., and D. Subrahmanyam, 1982: The 30–50 day mode at 850 mb during MONEX. *J. Atmos. Sci.*, **39**, 2088–2095.
- , D. N. Chakraborty, N. Cubukcu, L. Stefanova, and T. S. V. Vijaya Kumar, 2003: A mechanism of the MJO based on interactions in the frequency domain. *Quart. J. Roy. Meteor. Soc.*, **129**, 2559–2590.
- Lacis, A. A., and J. E. Hansen, 1974: A parameterization for the absorption of solar radiation in the earth's atmosphere. *J. Atmos. Sci.*, **31**, 118–133.
- Lau, K. M., and P. H. Chan, 1986: Aspects of the 40–50 day oscillation during the northern summer as inferred from outgoing longwave radiation. *Mon. Wea. Rev.*, **114**, 1354–1367.
- Liebmann, B., and C. A. Smith, 1996: Description of a complete (interpolated) outgoing longwave radiation dataset. *Bull. Amer. Meteor. Soc.*, **77**, 1275–1277.
- , G. N. Kiladis, J. A. Marengo, T. Ambrizzi, and J. D. Glick, 1999: Submonthly convective variability over South America and the South Atlantic convergence zone. *J. Climate*, **12**, 1877–1891.
- Maloney, E. D., and J. T. Kiehl, 2002: MJO-related SST variations over the tropical eastern Pacific during Northern Hemisphere summer. *J. Climate*, **15**, 675–689.
- Mellor, G. L., and T. Yamada, 1982: Development of a turbulence closure model for geophysical fluid processes. *Rev. Geophys. Space Phys.*, **20**, 851–875.
- Misra, V., 2004: An evaluation of the predictability of austral summer season precipitation over South America. *J. Climate*, **17**, 1161–1175.
- , and M. Kanamitsu, 2004: Anomaly nesting: A methodology to downscale seasonal climate simulations from AGCMs. *J. Climate*, **17**, 3249–3262.
- , P. A. Dirmeyer, and B. P. Kirtman, 2002a: A comparative study of two land surface schemes in regional climate integrations over South America. *J. Geophys. Res.*, **107**, 8080, doi:10.1029/2001JD001284.
- , —, —, H.-M. H. Juang, and M. Kanamitsu, 2002b: Regional simulation of interannual variability over South America. *J. Geophys. Res.*, **107**, 8036, doi:10.1029/2001JD900216.
- , —, and —, 2003: Dynamic downscaling of regional climate over South America. *J. Climate*, **16**, 103–117.
- Miyakoda, K., and J. Sirutis, 1977: Comparative integrations of global models with various parameterized processes of sub-grid-scale vertical transports: Description of the parameterizations. *Beitr. Phys. Atmos.*, **50**, 445–487.
- Mohr, K. I., and E. J. Zipser, 1996: Mesoscale convective systems defined by their 85-GHz ice scattering signature: Size and intensity comparison over tropical oceans and continents. *Mon. Wea. Rev.*, **124**, 2417–2437.
- Moorthi, S., and M. J. Suarez, 1992: Relaxed Arakawa–Schubert: A parameterization of moist convection for general circulation models. *Mon. Wea. Rev.*, **120**, 978–1002.
- Murakami, M., 1979: Large-scale aspects of deep convective activity over the GATE area. *Mon. Wea. Rev.*, **107**, 994–1012.
- Paegle, J. N., and K. C. Mo, 1997: Alternating wet and dry conditions over South America during summer. *Mon. Wea. Rev.*, **125**, 279–291.
- , L. A. Byerle, and K. C. Mo, 2000: Intraseasonal modulation of South American summer precipitation. *Mon. Wea. Rev.*, **128**, 837–850.
- Pan, H.-L., and L. Mahrt, 1987: Interaction between soil hydrology and boundary layer developments. *Bound.-Layer Meteor.*, **38**, 185–202.
- , and W.-S. Wu, 1995: Implementing a mass flux convective

- parameterization package for the NMC Medium-Range Forecast model. NMC Office Note 409, 40 pp. [Available from NOAA/NWS/NCEP, Environmental Modeling Center, WWB, Room 207, Washington, DC 20233.]
- Reynolds, R. W. A., and T. M. Smith, 1994: Improved global sea surface temperature analyses using optimum interpolation. *J. Climate*, **7**, 929–948.
- Ropelewski, C. F., and S. M. Halpert, 1987: The global climate for June–August 1986: Dry conditions plague parts of the Northern Hemisphere. *Mon. Wea. Rev.*, **115**, 705–720.
- Slingo, J. M., 1987: Development and verification of a cloud prediction scheme for the ECMWF model. *Quart. J. Roy. Meteor. Soc.*, **113**, 899–927.
- , and Coauthors, 1996: Intraseasonal oscillations in 15 atmospheric general circulation models: Results from an AMIP diagnostic subproject. *Climate Dyn.*, **12**, 325–357.
- Sperber, K. R., and Coauthors, 2001: Dynamical seasonal predictability of the Asian summer monsoon. *Mon. Wea. Rev.*, **129**, 2226–2248.
- Tiedtke, M., 1984: The effect of penetrative cumulus convection on the large-scale flow in a general circulation model. *Beitr. Phys. Atmos.*, **57**, 216–239.
- Velasco, I., and J. M. Fritsch, 1987: Mesoscale convective complexes in the Americas. *J. Geophys. Res.*, **92** (D8), 9591–9613.
- Waliser, D. E., and Coauthors, 2003a: AGCM simulations of intraseasonal variability associated with the Asian summer monsoon. *Climate Dyn.*, **21**, 423–446.
- , K. M. Lau, W. Stern, and C. Jones, 2003b: Potential predictability of the Madden–Julian oscillation. *Bull. Amer. Meteor. Soc.*, **84**, 33–50.
- Xue, Y.-K., P. J. Sellers, J. L. Kinter, and J. Shukla, 1991: A simplified biosphere model for global climate studies. *J. Climate*, **4**, 345–364.
- , F. J. Zeng, and C. A. Schlosser, 1996: SSiB and its sensitivity to soil properties: A case study using HAPEX-Mobilhy data. *Global Planet. Change*, **13**, 183–194.
- Yang, G.-Y., and J. Slingo, 2001: The diurnal cycle in the Tropics. *Mon. Wea. Rev.*, **129**, 784–801.
- Zheng, Y., D. E. Waliser, W. F. Stern, and C. Jones, 2004: The role of coupled sea surface temperatures in the simulation of the tropical intraseasonal oscillation. *J. Climate*, **17**, 4109–4134.
- Zhou, J., and K.-M. Lau, 1998: Does a monsoon climate exist over South America? *J. Climate*, **11**, 1020–1040.